J Med Ultrasonics
DOI 10.1007/s10396-014-0574-4

ORIGINAL ARTICLE

Accurate ultrasound imaging based on range point migration method for the depiction of fetal surface

Hirofumi Taki · Shinya Tanimura · Takuya Sakamoto · Tsuyoshi Shiina · Toru Sato

Received: 14 May 2014 / Accepted: 18 August 2014

Abstract
Purpose The purpose of this study is to evaluate the performance of a modified range point migration (RPM) method using a semi-broad transmit beam for fetal surface imaging.
Methods The conventional RPM method depicts accurate images of target surfaces by estimating the reflection point on a target surface from the path length of plural transmit-and-receive element combinations. However, the conventional RPM method depicts false images when echoes from different targets are received simultaneously. For the elimination of false images in the employment of the RPM method, we propose a modified RPM method with a semi-broad transmit beam to decrease the number of targets in each measurement region.
Results The modified RPM method depicted two acrylic cylinders of 2 cm in diameter with a root-mean-square error (RMSE) of 0.062 mm, where the RMSE of the migration method was 0.145 mm. The modified RPM method also succeeded in depicting a 7-month fetal phantom with a RMSE of 0.058 mm relative to a 3D image acquired using optical measurement.
Conclusion This study shows the potential of the modified RPM method in achieving accurate surface imaging of multiple targets using a semi-broad beam, indicating that the method is suitable for fetal surface imaging.

H. Taki (✉) · T. Sakamoto · T. Shiina · T. Sato
Graduate School of Informatics, Kyoto University, Yoshida-honmachi, Sakyo-ku, Kyoto 606-8501, Japan
e-mail: hirofumi.taki@mb6.seikyou.ne.jp

S. Tanimura
Furuno Electric Co., Ltd, 9-52 Ashihara-cho, Nishinomiya, Hyogo 662-8580, Japan

Keywords Three-dimensional ultrasonography · Fetal imaging · Fetal surface · Range point migration · Migration

Introduction

Three-dimensional (3D) ultrasonography imaging has been developed to evaluate tissue structure, for example the measurement of organ and tumor volume [1–4]. In perinatal medicine, 3D ultrasound has become a common procedure for the examination of fetal anatomy because of its safety and low cost [5–7]. However, 3D fetal ultrasound images acquired using surface rendering have inadequate image quality [8–10]. In addition, the conventional high-resolution ultrasound imager requires the use of a focused transmit beam. For the improvement of safety in fetal imaging, use of a broad transmit beam is preferable. Therefore, an accurate ultrasound imaging method using a broad transmit beam is desirable for the evaluation of fetal development.

We have previously reported on several high-resolution or high-accuracy ultrasound imaging methods [11–13]; however, they employed a focused transmit beam and are unsuitable for the depiction of the fetal surface. Several researchers have evaluated ultrasound imaging methods using broad transmit beams, and most of them have focused on the improvement of temporal resolution [14–18]. The delay-and-sum migration method has been widely used in ultrasound imaging, where the basic technique was first reported in the 1950s [19]. The migration method integrates all of the received data coherently by summation along hyperbolic trajectories, and the migration image obtained using a broad transmit beam has a similar quality to that obtained using a narrow transmit beam. Several researchers have reported on ultrasound imaging methods based on the migration method [20–22]; however, these

Published online: 13 September 2014

methods exhibited little improvement in spatial resolution over the conventional migration method.

The envelope method has been proposed for the acquisition of an accurate 3D image of a target surface using a broad transmit beam [23, 24]. The method depicts an ellipse for each transmit-and-receive element combination, where its foci are the transmit and receive elements and the length of its long axis is equal to the path length. The target surface is estimated by means of the envelope of the ellipses. Because the envelope image becomes inaccurate when multiple targets exist in the region of interest (ROI), Kidera et al. [25] studied the range point migration (RPM) method for the depiction of accurate images of multiple target surfaces. The RPM method also employs a broad transmit beam, and depicts an ellipse for each transmit-and-receive element combination. The difference between the RPM method and the envelope method is that the RPM method determines the target position on the ellipse from the path length of plural transmit-and-receive element combinations. This process enables the RPM method to depict the images of target surfaces under the condition that multiple targets exist in the ROI. However, when multiple echoes from different targets are received simultaneously, the RPM method fails to estimate the target position and false images appear.

In our previous studies, we reported on the above-mentioned problem regarding the RPM method, and indicated the possibility that use of a broad transmit beam could solve this problem [26, 27]. In the current study, we investigate the performance of a modified RPM method using a semi-broad transmit beam in an experimental study using acrylic cylinders and a fetal phantom.

Materials and methods

To improve the safety of 3D fetal ultrasonography, we employ a semi-broad transmit beam. The migration method has been widely employed in ultrasound imaging, and it can use a semi-broad transmit beam. We thus compare the performance of the modified RPM method involving use of a semi-broad beam to that of the migration method. In this section, we first describe the schema of the migration method. Next, we report the principle of the conventional RPM method and its weakness in instances where there are multiple targets in the ROI. We propose a technique using a semi-broad transmit beam to depict target surfaces in cases where multiple targets exist. We describe the experimental setup in the final sub-section.

Migration method

The migration method estimates the intensity at the measurement position by means of summation along the hyperbolic trajectory. All the received signals shifted by appropriate path lengths are superimposed to focus at each measurement point. The estimated intensity at a measurement point is calculated by the following formula:

$$S(\mathbf{r}) = \left| \sum_{i,j} s_{i,j}(|\mathbf{x}_i - \mathbf{r}|/c + |\mathbf{x}_j - \mathbf{r}|/c) \right|^2, \quad (1)$$

where $\mathbf{r}$ denotes the position vector of the measurement point, $s_{i,j}(t)$ denotes the received signal of the combination of the i-th transmit element, and j-th receive element after the filtering process using a matched filter at the time of flight of t. $\mathbf{x}_i$ denotes the position vector of the i-th element X_i and c is the sound velocity. The impulse response of the matched filter used in this study is given by:

$$p(t) = \exp\left(-t^2/2\sigma_M^2\right)\cos(\omega_C t), \quad (2)$$

where σ_M is a constant and ω_C is the angular frequency at the transmit center frequency [24]. In the current study, we set σ_M as 0.4 μs.

Principle of RPM method

Figure 1 shows the schema of the RPM method. The RPM method is based on a simple fundamental assumption that the reflection point on the target surface is located on an ellipse, where the foci are the position of a transmit element and that of a receive element and the length of its long axis is the path length [25]. The path length of each transmit-and-receive combination is determined from the peak intensity position of the received signal after applying a matched filter. The RPM method estimates the reflection point on an ellipse using the intersections of several ellipses. The RPM method assumes that the direction of the

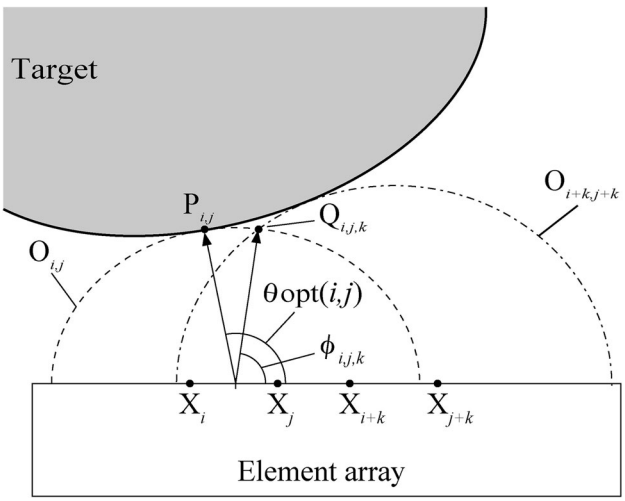

Fig. 1 Schema for estimation of the reflection point on a target surface using the range point migration method

reflection point should be close to that of the intersection of the ellipses determined by echo delay. Therefore, the RPM method employs a weighting function whose value decreases in response to the difference between the estimated direction of the reflection point and the direction of an intersection. For the estimation of the direction of the reflection point at the combination of the i-th transmit element X_i and the j-th receive element X_j, we employ a weighting function given by:

$$f(\theta,i,j,k)=\exp\left[-\frac{\{\theta-\phi_{i,j,k}\}^2}{2\sigma_\theta^2}\right], \tag{3}$$

where θ is a candidate direction of the reflection point $P_{i,j}$ located on the ellipse $O_{i,j}$, k is an integer except 0, $\phi_{i,j,k}$ is the direction of the intersection $Q_{i,j,k}$ between the ellipses $O_{i,j}$ and $O_{i+k,j+k}$, and σ_θ is a constant. In the current study, we set $\sigma_\theta = 1^\circ$ and $1 \le k \le 6$.

The RPM method introduces two assumptions to estimate the direction of the reflection point. First, the directions of intersections should be concentrated to the direction of the reflection point. Second, the difference between the direction of the reflection point and that of an intersection should increase as the center distance between two ellipses increases. The RPM method estimates the direction of arrival $\theta_{\mathrm{OPT}}(i, j)$ by means of the following formulae [25]:

$$\theta_{\mathrm{OPT}}(i,j)=\arg\max_\theta F(\theta,i,j), \tag{4}$$

$$F(\theta,i,j)=\left|\sum_k s_{i+k,j+k}(T_{i+k,j+k})f(\theta,i,j,k)\exp\left[-\frac{d_k^2}{2\sigma_X^2}\right]\right|, \tag{5}$$

where $F(\theta, i, j)$ is the evaluation function at the candidate direction of arrival θ for the combination of the i-th transmit element and the j-th receive element, $cT_{i,j}$ is the path length for the combination of the i-th transmit element and the j-th receive element, d_k is the center distance between the ellipses $O_{i,j}$ and $O_{i+k,j+k}$, and σ_X is a constant. Because the value of $f(\theta, i, j, k)$ decreases as the difference between θ and $\phi_{i,j,k}$ increases, the employment of $f(\theta, i, j, k)$ enables the RPM method to select the direction where intersections are concentrated to the direction of the reflection point. The exponential term in Eq. (5) emphasizes the contribution of the intersections of ellipses close to $O_{i,j}$. In the current study, we set σ_X as twice the wavelength at the transmit center frequency.

When two ellipses are bound on different targets, the intersection between the two ellipses causes the appearance of a false image, as shown in Fig. 2. Under the condition where there is a false image, the evaluation function $F(\theta, i, j)$ has multiple local maximum values for the directions of the true reflection points and that of the false image.

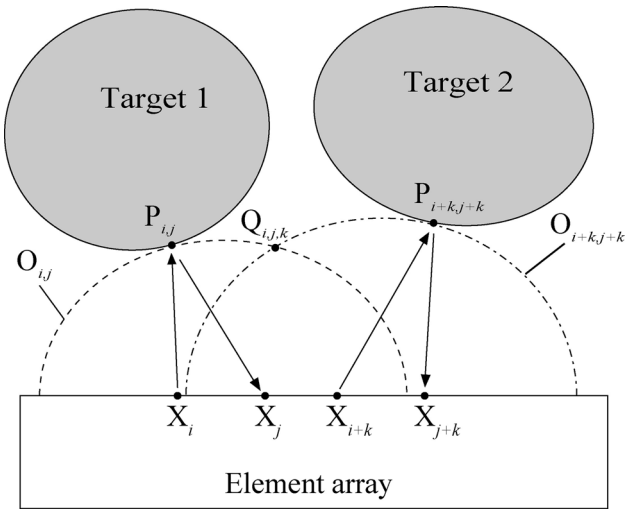

Fig. 2 Appearance of false images with the range point migration method in the presence of multiple targets

Therefore, our previous study eliminated the transmit-and-receive combination whose evaluation function satisfied the following formula [26]:

$$F(\theta_1,i,j)/2<F(\theta_2,i,j), \tag{6}$$

where θ_1 and θ_2 are the directions of the greatest maximum value and the second local maximum value, respectively. The introduction of this process succeeded in eliminating false images at the cost of some missing regions in the images of target surfaces [26].

Modified RPM method using semi-broad transmit beam

In the RPM method, false images or missing regions appear when multiple targets exist in the measurement region. Therefore, we employ a semi-broad transmit beam to suppress the number of targets in each measurement region, as shown in Fig. 3. Because the RPM method has been proposed under the condition of employing a hemisphere transmit beam, we propose a modified RPM method using a semi-broad transmit beam.

The employment of a semi-broad transmit beam affects the intensity of the received signal. We compensate for the effect of the transmit-beam directivity on the signal intensity. The received signal after compensation, $s_{\mathrm{B}m,i,j,k}(t)$, is calculated using the following formula:

$$s_{\mathrm{B}m,i,j,k}(t)=\frac{s'_{i+k,j+k}(t)}{B_m(\phi_{i,j,k}-\varepsilon_m)}, \tag{7}$$

where $s'_{i,j}(t)$ denotes the received signal using the combination of the i-th transmit element and j-th receive element after the filtering process using the matched filter, B_m is the m-th transmit-beam pattern, and ε_m is the focal direction of the m-th transmit beam. Figure 4 shows a transmit-beam

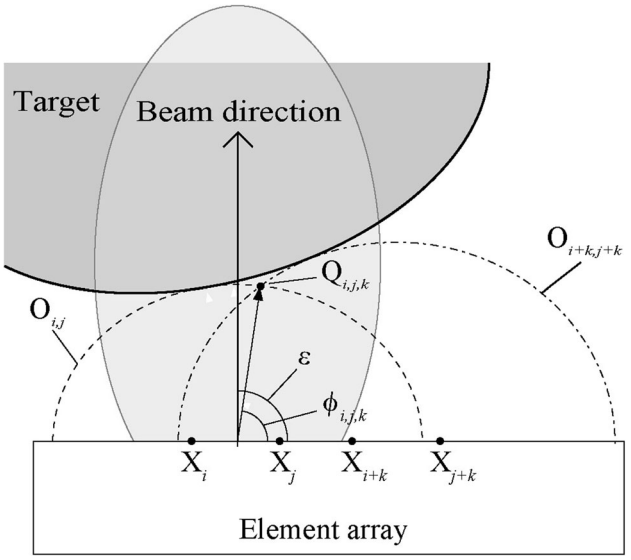

Fig. 3 Employment of a semi-broad beam to avoid the condition under which echoes from different targets are received simultaneously

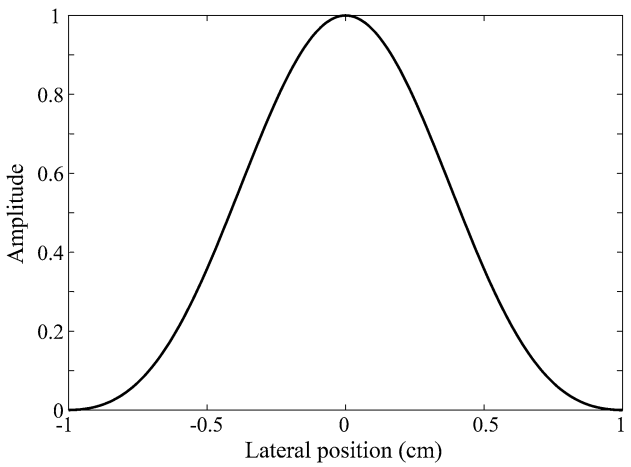

Fig. 4 Transmit-beam pattern at a depth of 5 cm constructed from the received data of seven adjacent transmit elements using the synthetic aperture technique, where the amplitude after applying a matched filter at each lateral position is normalized by the maximum amplitude. The element pitch is 0.6 mm, and the focus is located at the center

pattern, B_m, at a depth of 5 cm, where its focus is located at the center. This pattern indicates that the employment of the semi-broad transmit beam suppresses the width of each measurement region to less than 1.5 cm. Because the center distance of the two 2-cm-diameter cylinders was 2 cm, use of the semi-transmit beam might have effectively avoided the condition where multiple echoes from different targets were received.

The direction of arrival estimated using the modified RPM method, $\theta_{\mathrm{BOPT}}(i, j)$, is given by the following formulae:

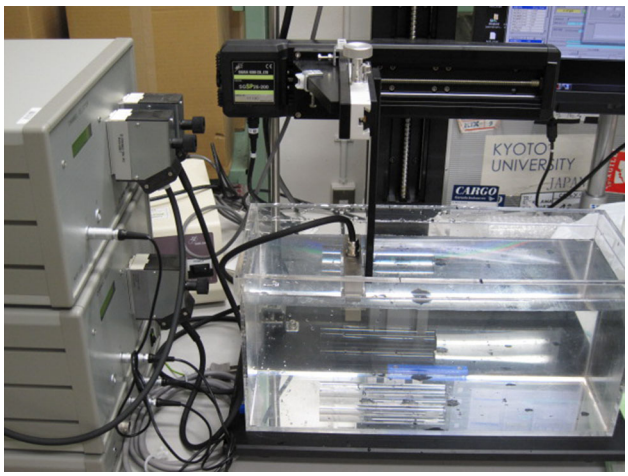

Fig. 5 Picture of the experimental setup used in the current study

$$\theta_{\mathrm{BOPT}}(i,j) = \arg\max_{\theta} F_{\mathrm{B}m}(\theta,i,j), \tag{8}$$

$$F_{\mathrm{B}m}(\theta,i,j) = \left|\sum_{k} s_{\mathrm{B}m,i,j,k}(T_{i+k,j+k}) f(\theta,i,j,k) \exp\left[-\frac{d_k^2}{2\sigma_X^2}\right]\right|, \tag{9}$$

where $F_{\mathrm{B}m}(\theta, i, j)$ is the evaluation function of the modified RPM method at the candidate direction of arrival θ for the combination of the i-th transmit element and the j-th receive element. The RPM method estimates the reflection points distributed on target surfaces. We use a resampling technique to construct the image of the target surfaces from the reflection points acquired using the modified RPM method. The estimated intensity at a measurement point using the modified RPM method is given by:

$$P_{\mathrm{B}}(\mathbf{u}) = \sum_{m}\sum_{i,j} s_{\mathrm{BOPT}m,i,j}(T_{i,j}) \exp\left[-\frac{\left|\mathbf{u}-\mathbf{R}_{i,j}\right|^2}{2\sigma_{\mathrm{I}}^2}\right], \tag{10}$$

$$s_{\mathrm{BOPT}m,i,j}(t) = \frac{s'_{i,j}(t)}{B_m[\theta_{\mathrm{BOPT}}(i,j)-\varepsilon_m]}, \tag{11}$$

where $\mathbf{u}$ and $\mathbf{R}_{i,j}$ are the position vectors of a measurement point and a reflection point, respectively. In the current study, we set the grid size and σ_{I} as 0.3 and 0.2 mm, respectively.

Experimental Setup

Figures 5 and 6 show a picture and the schema of the experimental system used in the current study, respectively. For simplicity, we evaluated the performance of the modified RPM method in two-dimensional experiments. We used a concave element array, which consists of 128 elements without an acoustic lens, with a curvature radius

of 50 mm and an element pitch of 0.6 mm. The size of each element is 0.5 mm by 10 mm in the lateral and elevation directions, respectively. A single element transmitted a double-cycle pulse with a center frequency of 2.0 MHz at a time. All elements received the echoes, where the sampling frequency was 10 MHz.

Because the experimental system activated a single transmit element at a time, we employed the synthetic aperture technique to construct a virtual transmit beam [28–30]. The received signal using a synthesized semi-broad transmit beam is given by:

$$s'_{i,j}(t) = \sum_h s_{h,j}\left(t - \frac{\left|\overrightarrow{F_m X_h}\right| - \left|\overrightarrow{F_m X_i}\right|}{c}\right), \tag{12}$$

where F_m is the position of the m-th focal point. In the modified RPM method using all of the 128 elements, the received data from seven adjacent transmit elements were synthesized to construct a transmit beam. We also investigated the performance of the proposed and conventional methods using a sparse array [31–33]. For this purpose, we used 32 sparse elements out of all 128 elements, where the element pitch increased to 2.4 mm. In the modified RPM method using 32 sparse elements, the received data from three transmit elements were synthesized to construct a transmit beam.

We used two acrylic cylinders and a fetal phantom to evaluate the performance of the modified RPM method. The two acrylic cylinders were contiguous to each other, where the diameter of each cylinder was 2.0 cm. The fetal phantom was modeled on a 7-month fetus (3B Scientific GmbH, Hamburg, Germany). In the experiment using a fetal phantom, we also measured the phantom by means of the optical 3D digitizer VIVID 910 (Konica Minolta Inc., Tokyo, Japan) to evaluate the accuracy of the modified RPM method in depicting the fetal phantom. The digitizer had a spatial resolution of 8 μm. Because we used a transducer with no acoustic lens, in the experiment using a fetal phantom, it was not guaranteed that the reflection point would be present in the measurement plane. Therefore, we constructed the target boundary from the 3D image acquired by the digitizer. First, we selected a reflection point, P_{Di}, on the surface of the fetal phantom acquired by the digitizer for each element, X_i, where the distance between the element position and the point on the surface of the fetal phantom was minimal at P_{Di}. We then transferred the reflection point, $\mathbf{R}_{Di}$, to the degenerate point in the measurement plane, P_{Di}', as shown in Fig. 7. P_{Di}' satisfied the following formulae:

$$r_{Dix} = r'_{Dix}, \tag{13}$$

$$|\mathbf{R}_{Di} - \mathbf{x}_i| = |\mathbf{R}'_{Di} - \mathbf{x}_i|, \tag{14}$$

where r_{Dix} and r_{Dix}' are the lateral position of P_{Di} and P_{Di}', respectively, and $\mathbf{R}_{Di}$ and $\mathbf{R}_{Di}$' are the position vector of P_{Di} and P_{Di}', respectively. We calculated the distance between the surface boundary of the fetal phantom acquired by the modified RPM method and the boundary depicted by P_{Di}'.

In evaluating the performance of the proposed method, we used the boundary of the imaging methods with an estimated intensity higher than −20 dB of the peak estimated intensity in the ROI. We calculated the root-mean-square error (RMSE) of the acquired boundary e given by:

$$e = \min_{\psi,\mathbf{n}} \sqrt{\frac{\sum_k P(k)\left|\overrightarrow{\mathrm{U}_k C(\psi, \mathbf{n}, \mathrm{U}_k)}\right|^2}{\sum_k P(k)}}, \tag{15}$$

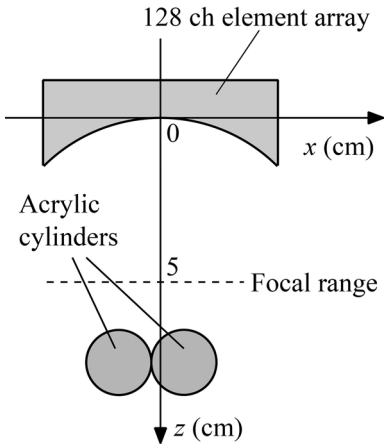

Fig. 6 Schema of the ultrasound measurement system used in the two-cylinder experiment

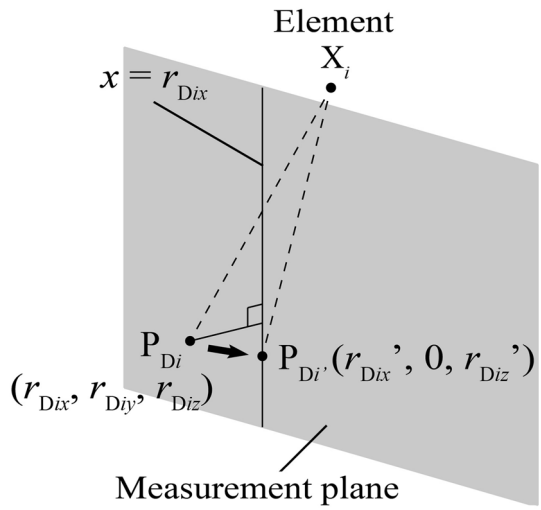

Fig. 7 Construction of the surface boundary of a fetal phantom from the 3D image acquired by a 3D digitizer. P_{Di} is the point on the acquired 3D fetal surface that is closest to element X_i. P_{Di}' is the degenerate point in the measurement plane transferred from point P_{Di}

where ψ and **n** are the rotation angle and the vector for the parallel movement to adjust the true boundary to the estimated boundary, respectively, U_k is the k-th point on the boundary, $P(k)$ is the estimated intensity at U_k, and $C(\psi, \mathbf{n}, U_k)$ is the point on the true boundary after adjustment that is closest to the boundary point, U_k. In the experiment using two 2-cm-diameter cylinders, we used two 2-cm-diameter circles that were contiguous to each other as the true boundary. In the experiment using a fetal phantom, we used the boundary acquired by a 3D digitizer as the true boundary.

Results

Figures 8 and 9 show the images of two acrylic cylinders acquired using the migration method and the conventional RPM method using all of the 128 elements, respectively. The conventional RPM method depicted the target surface clearly as compared to the migration method; however, the conventional RPM image had missing regions at the tops of both cylinders, where the missing regions originated from the elimination process regarding false images as expressed in Eq. (6). In contrast, the modified RPM method using all of the 128 elements succeeded in depicting the two cylinders without a missing region, as shown in Fig. 10. RMSEs of the images acquired using the migration method, the conventional RPM method, and the modified RPM method were 0.145, 0.088, and 0.062 mm, respectively.

Figure 11 shows the images of two acrylic cylinders acquired using the migration method and the modified RPM method using a 32-element sparse array. The sparse array can reduce the number of elements; however, blind employment of the sparse array causes severe deterioration in image quality. In the migration image, the use of a sparse array thus caused the appearance of multiple false images. In contrast, the modified RPM method succeeded in clearly depicting the two acrylic cylinders. The RMSE of the image acquired using the modified RPM method was 0.068 mm. This result indicates that the modified RPM method is suitable for the accurate imaging of target surfaces using a sparse array and a semi-broad transmit beam.

The optical digitizer succeeded in depicting an accurate 3D image of a fetal phantom, as shown in Fig. 12. The white broken line indicates the ultrasound measurement plane. Figure 13 shows the ultrasound image of the fetal phantom in the measurement plane acquired by the modified RPM method, where the white broken curves represent the surface boundary of the fetal phantom calculated from the 3D digitizer image. The RMSE between the target surface acquired using the ultrasound measurement using the RPM method and that acquired using optical measurement using the 3D digitizer was 0.058 mm. The RMSE of the modified RPM method in the fetal experiment was similar to that in the cylinder experiment. This result supports the validity of the experimental study in the current report, and indicates the high potential regarding the application of the modified RPM method to 3D surface imaging of a fetus.

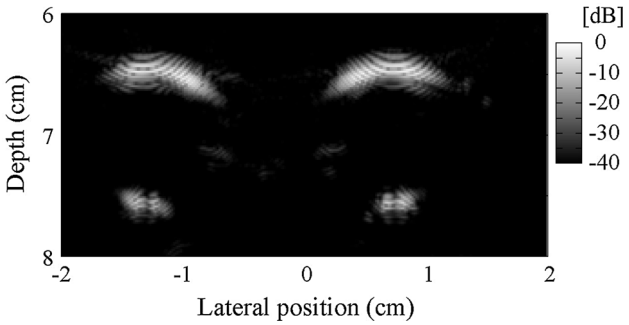

Fig. 8 Image of two acrylic cylinders acquired using the migration method, where the diameter of each cylinder is 2.0 cm. A 128-element array is employed

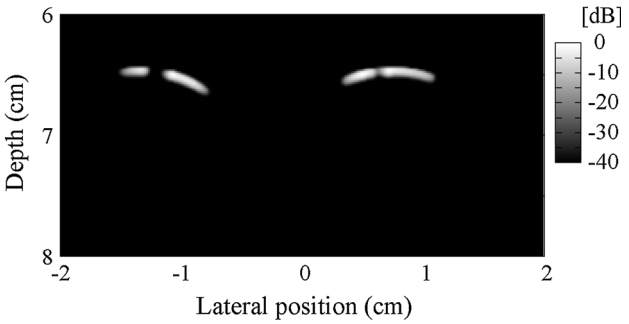

Fig. 9 Image of two acrylic cylinders acquired using the conventional range point migration method, where the diameter of each cylinder is 2.0 cm. A 128-element array is employed

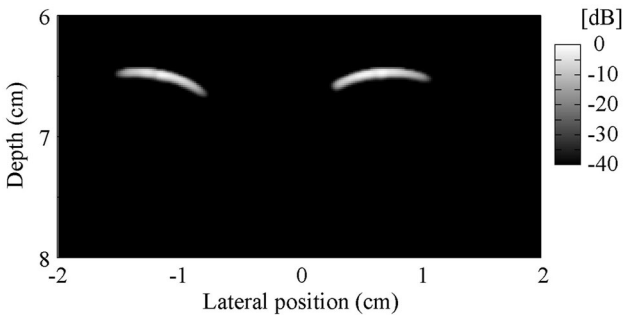

Fig. 10 Image of two acrylic cylinders acquired using the modified range point migration method, where the diameter of each cylinder is 2.0 cm. A 128-element array is employed

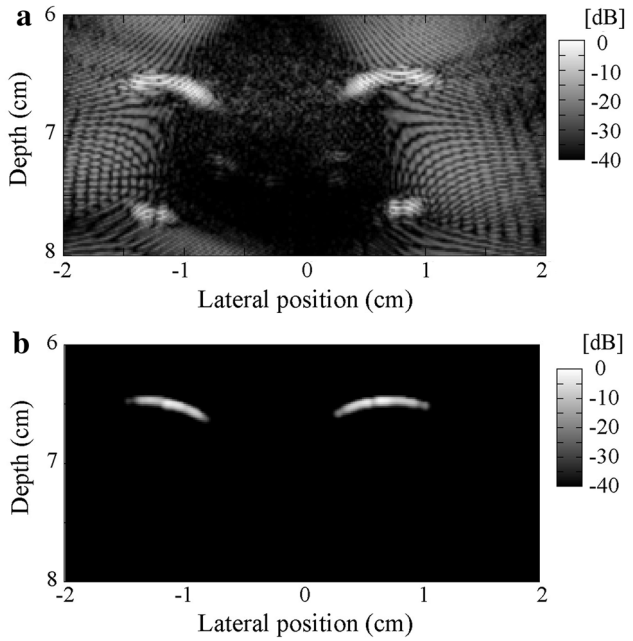

Fig. 11 Images of two acrylic cylinders acquired by the migration method (**a**) and by the modified range point migration method (**b**), where the diameter of each cylinder is 2.0 cm. A 32-element sparse array is employed

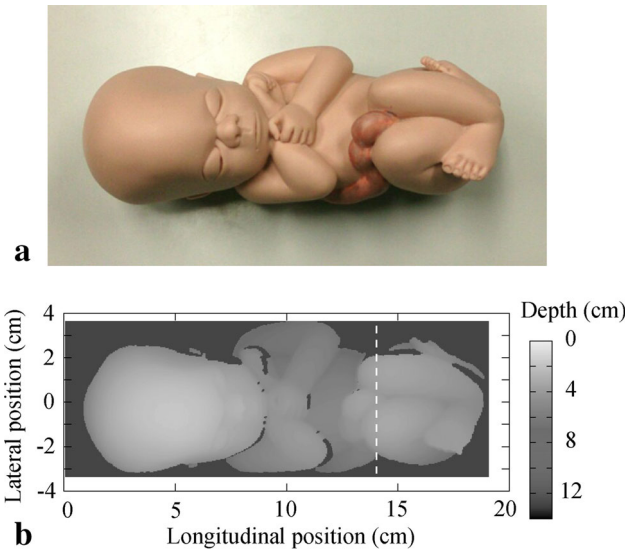

Fig. 12 Picture of a 7-month fetal phantom (**a**) and its 3D image acquired using an optical 3D digitizer (**b**). A *white broken line* indicates the ultrasound measurement plane

Conclusion

In the current study, we investigated the performance of the modified RPM method using a semi-broad transmit beam. The employment of a semi-broad transmit beam succeeded in removing the missing regions in the image acquired using the conventional RPM method. When a 128-element array transmitted ultrasound pulses at a 2.0-MHz center frequency, the modified RPM method depicted two acrylic cylinders of 2.0 cm in diameter with an RMSE of 0.062 mm, where the RMSE of the migration method was 0.145 mm. When a 32-element sparse array was employed, the RMSE of the modified RPM method was 0.068 mm in the depiction of the acrylic cylinders. Furthermore, the modified RPM method using a 128-element array depicted a 7-month fetal phantom with an RMSE of 0.058 mm as compared to the image acquired using an optical 3D digitizer. These results show the potential of the modified RPM method in achieving accurate imaging of the target surface using a sparse array and a semi-broad beam, indicating that the method may be suitable for fetal surface imaging.

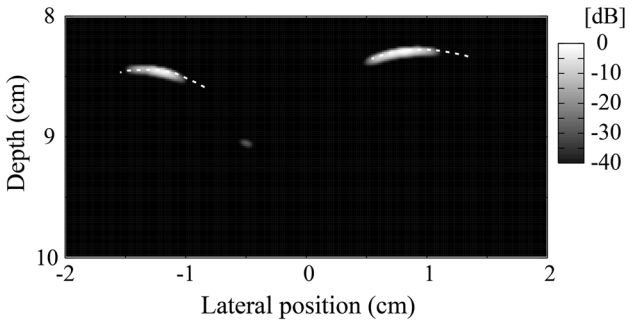

Fig. 13 Ultrasound image of a 7-month fetal phantom in a measurement plane acquired using the modified range point migration method. The *white broken curve* is the surface boundary of the fetal phantom calculated from the 3D digitizer image

The echoes from deeper-lying structures may cause the appearance of false images. However, we can suppress the appearance of false images by employing an additional weighting function concerning the time of flight, because the time of flight of the echo from a deeper-lying structure should be larger than that of the reflection point on the fetal surface. Future work should focus on expansion of the modified RPM method for the depiction of 3D targets, including the employment of a weighting function concerning the time of flight.

Acknowledgments This work is partly supported by the Innovative Techno-Hub for Integrated Medical Bio-Imaging of the Project for Developing Innovation Systems from the Ministry of Education, Culture, Sports, Science and Technology (MEXT), Japan, and by MEXT/JSPS KAKENHI Grant Number 25870345.

Conflict of interest Hirofumi Taki declares that he has no conflict of interest.Shinya Tanimura declares that he has no conflict of interest.Takuya Sakamoto declares that he has no conflict of interest.Tsuyoshi Shiina declares that he has no conflict of interest.Toru Sato declares that he has no conflict of interest.

Ethical considerations This article does not contain any studies with human or animal subjects performed by the any of the authors.

References

1. Nelson TR, Pretorius DH. Three-dimensional ultrasound imaging. Ultrasound Med Biol. 1998;24:1243–70.
2. Fenster A, Downey DB, Cardinal HN. Three-dimensional ultrasound imaging. Phys Med Biol. 2001;46:67–99.
3. Gee AH, Prager RW, Treece GM, et al. Engineering a freehand 3D ultrasound system. Pattern Recogn Lett. 2003;24:757–77.
4. Huang QH, Yang Z, Hu W, et al. Linear tracking for 3-D medical ultrasound imaging. IEEE Trans Cybern. 2013;43:1747–54.
5. Merz E. Current 3D/4D ultrasound technology in prenatal diagnosis. Eur Clin Obstet Gynecol. 2005;1:184–93.
6. Steen E, Olstad B. Volume rendering of 3D medical ultrasound data using direct feature mapping. IEEE Trans Med Imaging. 1994;13:517–25.
7. Varandas J, Baptista P, Santos J, et al. VOLUS: a visualization system for 3D ultrasound data. Ultrasonics. 2004;42:689–94.
8. Sakas G, Schreyer LA, Grimm M. Preprocessing and volume rendering of 3D ultrasonic data. IEEE Trans Vis Comput Graph. 1995;15:47–54.
9. Loizou CP, Pattichis CS, Christodoulou CI, et al. Comparative evaluation of despeckle filtering in ultrasound imaging of the carotid artery. IEEE Trans Ultrason Ferroelectr Freq Control. 2005;52:1653–69.
10. Wang SR, Sun YN, Chang FM. Artifact removal and texture-based rendering for visualization of 3D fetal ultrasound images. Med Biol Eng Comput. 2008;46:575–88.
11. Taki H, Sakamoto T, Yamakawa M, et al. Small calcification depiction in ultrasound B-mode images using decorrelation of echoes caused by forward scattered waves. J Med Ultasonics. 2011;38:73–80.
12. Taki H, Sakamoto T, Yamakawa M, et al. Small calcification indicator in ultrasonography using correlation of echoes with a modified Wiener filter. J Med Ultrason. 2012;39:127–35.
13. Taki H, Taki K, Sakamoto T, et al. High range resolution ultrasonographic vascular imaging using frequency domain interferometry with the Capon method. IEEE Trans Med Imaging. 2012;31:417–29.
14. Udesen J, Gran F, Hansen KL, et al. High frame-rate blood vector velocity imaging using plane waves: simulations and preliminary experiments. IEEE Trans Ultrason Ferroelectr Freq Control. 2008;55:1729–43.
15. Lu J. 2D and 3D high frame rate imaging with limited diffraction beams. IEEE Trans Ultrason Ferroelectr Freq Control. 1997;44:839–56.
16. Cheng J, Lu J. Extended high-frame rate imaging method with limited-diffraction beams. IEEE Trans Ultrason Ferroelectr Freq Control. 2006;53:880–99.
17. Hasegawa H, Kanai H. High-frame-rate echocardiography using diverging transmit beams and parallel receive beamforming. J Med Ultrason. 2011;38:129–40.
18. Hasegawa H, Kanai H. High-frame-rate echocardiography with reduced sidelobe level. IEEE Trans Ultrason Ferroelectr Freq Control. 2012;59:2569–75.
19. Hagedoorn JG. A process of seismic reflection interpretation. Geophys Prospect. 1954;2:85–127.
20. Cheng J, Lu J. Extended high-frame rate imaging method with limited-diffraction beams. IEEE Trans Ultrason Ferroelectr Freq Control. 2006;53:880–99.
21. Garcia D, Tarnec LL, Muth S, et al. Stolt's f-k migration for plane wave ultrasound imaging. IEEE Trans Ultrason Ferroelectr Freq Control. 2013;60:1853–67.
22. Gray SH, Etgen J, Dellinger JJ, et al. Seismic migration problems and solutions. Geophysics. 2001;66:1622–40.
23. Kidera S, Sakamoto T, Sato T. High-resolution and real-time UWB radar imaging algorithm with direct waveform compensations. IEEE Trans Geosci Remote Sens. 2008;46:3503–13.
24. Sakamoto T, Taki H, Sato T. An experimental study of ultrasonic imaging with a reduced number of array elements using the envelope method. Acoust Sci Tech. 2011;32:143–50.
25. Kidera S, Sakamoto T, Sato T. Accurate UWB radar three-dimensional imaging algorithm for a complex boundary without range point connections. IEEE Trans Geosci Remote Sens. 2010;48:1993–2004.
26. Tanimura S, Taki H, Sakamoto T, et al. Accurate ultrasound imaging of the surface of an embryo using Range Point Migration method—Suppression of false images using transmit directivity—(in Japanese). In: Proceedings. Research Committee on Basic Technologies in Ultrasonics in Medicine. 2012;BT2012-08:14–9.
27. Taki H, Tanimura S, Sakamoto T, et al. Accurate ultrasound imaging of the surface of a fetus using a broad ultrasound beam. In: Proceedings. XXIV European Congress of Perinatal Medicine. 2014, accepted.
28. Frazier CH, O'Brien WD. Synthetic aperture techniques with a virtual source element. IEEE Trans Ultrason Ferroelectr Freq Control. 1998;45:196–207.
29. Nikolov SI, Sant'en P, Bjuvsten O, et al. Parameter study of 3-D synthetic aperture post-beamforming procedure. Ultrasonics. 2006;44:e159–64.
30. Andresen H, Nikolov SI, Pedersen MM, et al. Three-dimensional synthetic aperture focusing using a rocking convex array transducer. IEEE Trans Ultrason Ferroelectr Freq Control. 2010;57:1051–63.
31. Weber PK, Schmitt RM, Tylkowski BD, et al. Optimization of random sparse 2D-transducer arrays for 3D electronic steering and focusing. Proc IEEE Int Ultrason Symp. 1994;3:1503–6.
32. Lockwood GR, Foster FS. Optimizing the radiation pattern of sparse periodic two-dimensional arrays. IEEE Trans Ultrason Ferroelectr Freq Control. 1996;43:15–9.
33. Holm S, Elgetun B, Dahl G. Properties of the beampattern of weight- and layout-optimized sparse arrays. IEEE Trans Ultrason Ferroelectr Freq Control. 1997;44:983–91.